Analytical strategies to evaluate the in-depth degradation processes in protein-based heritage substrates exposed to ion beam techniques

M. Ma[1], Z. Li[1], G. Sciutto[1], M. Zangari[2], T. Salzillo[2], E. Venuti[2], Z. Szikszai[3], B. Döncző[3], S. Prati[1*]

[1] *Microchemical and Microscopy Art Diagnostic Laboratory, Department of Chemistry, University of Bologna, Department of Chemistry-Ravenna Campus, Via Guaccimanni 42, 48121, Ravenna, Italy*

[2] *Molecular Spectroscopy Group, Department of Industrial Chemistry, University of Bologna, Via Gobetti 85, 40129, Bologna, Italy*

[3] *HUN-REN Institute for Nuclear Research (ATOMKI), Bem tér 18/c, H-4026 Debrecen, Hungary*

SUPPLEMENTARY

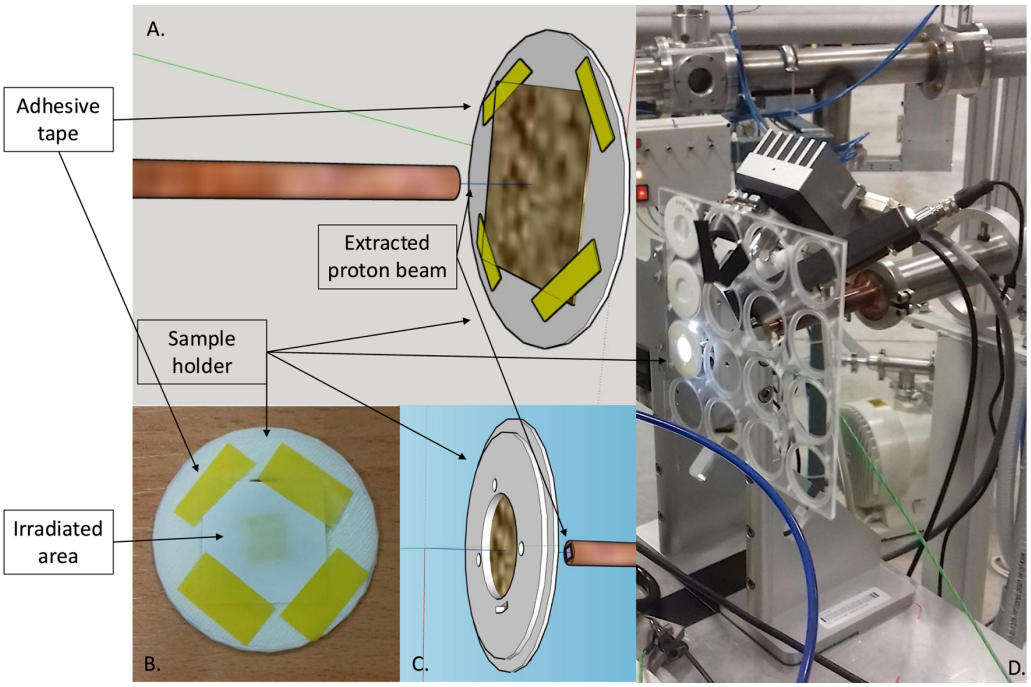

Figure S1. Schematic demonstration of proton beam irradiation geometry. Panel A & C are CAD models of the sample, the holder and the irradiation geometry; Panel B is an image of an irradiated sample, still fixed in place using adhesive tapes; Panel D shows the milli-beam irradiation setup with 3 samples loaded.

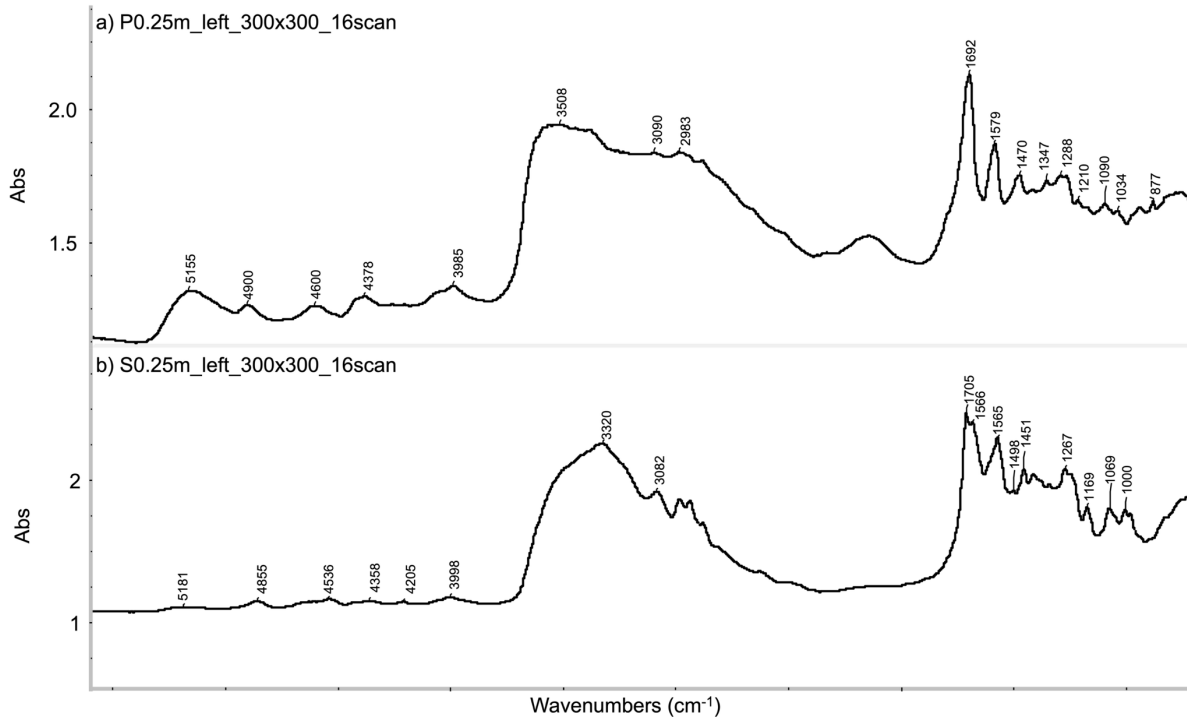

Figure S2. NIR and MID spectra of (a) pristine parchment (b) pristine silk

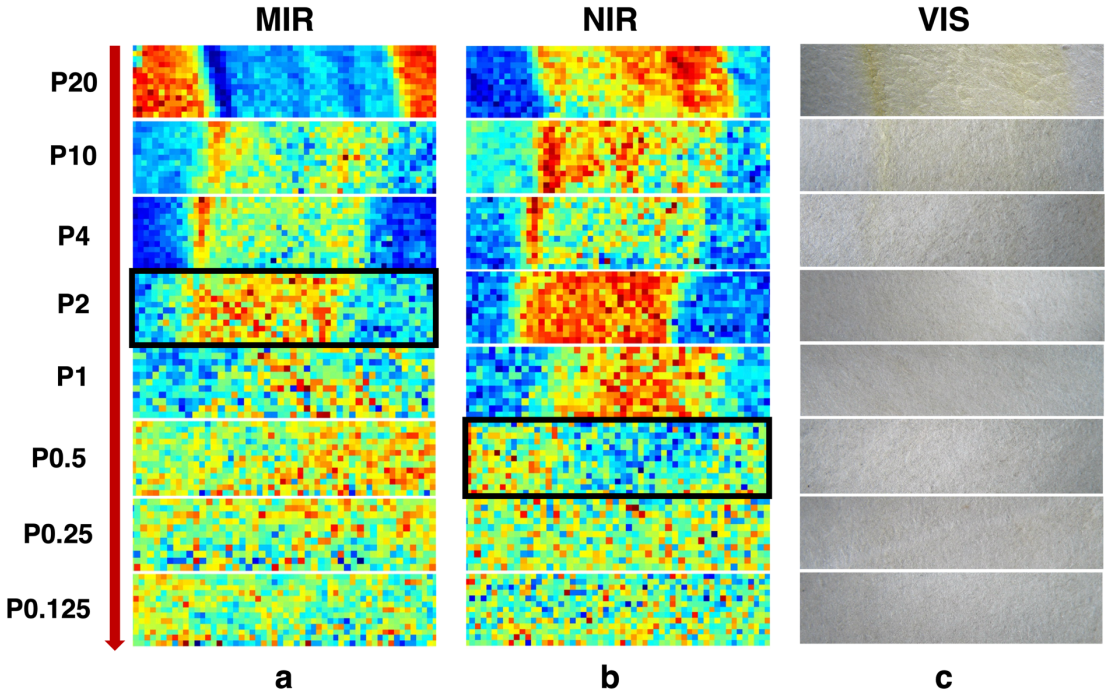

Figure S3. Parchment degradation patterns identified in selected PCA score maps (a, b) with corresponding visible images (c) captured via stereomicroscopy. Black rectangles indicate the detection threshold within the MIR (a) and NIR regions (b).

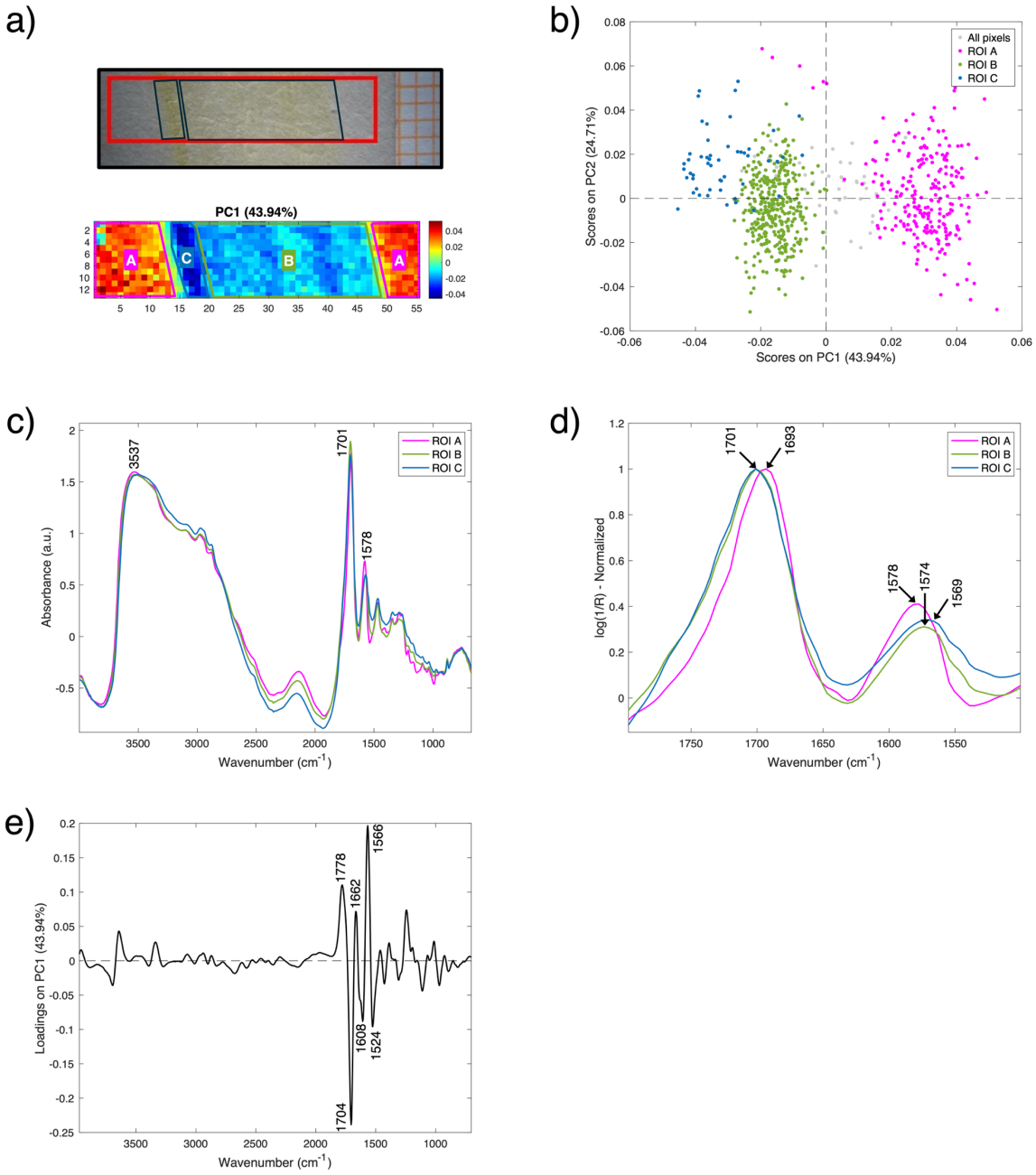

Figure S4. PCA brushing results of P20 on PC1 score map with a focus on selected MIR region (1800–1500 cm^{-1}). (a) FTIR mapping area indication on visible image and PC1 score map brushing areas of P20; (b) highlighted scores in PCA score plot of three clusters: unirradiated area (A); irradiated area (B); potential grouping (C); (c) corresponding average spectra with (d) normalized region enlargement based on amide I; (e) PC1 loading profile from the first derivative PCA model.

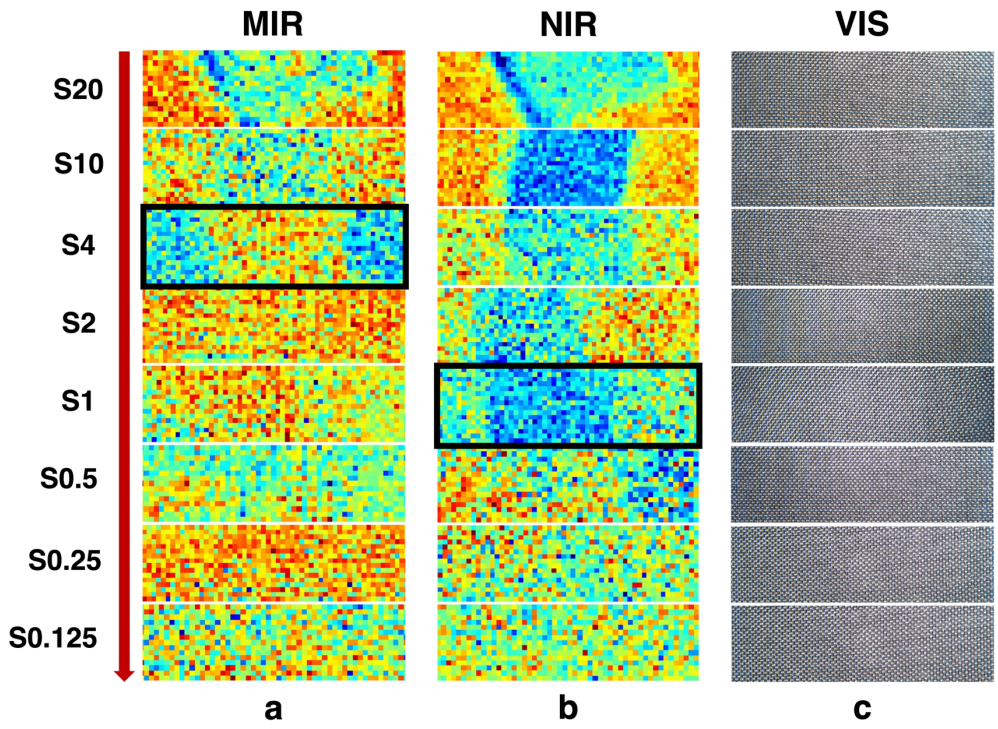

Figure S5. Silk degradation patterns identified in selected PCA score maps (a, b) with corresponding visible images (c) captured via stereomicroscopy. Black rectangles indicate the detection threshold within the MIR (a) and NIR regions (b).

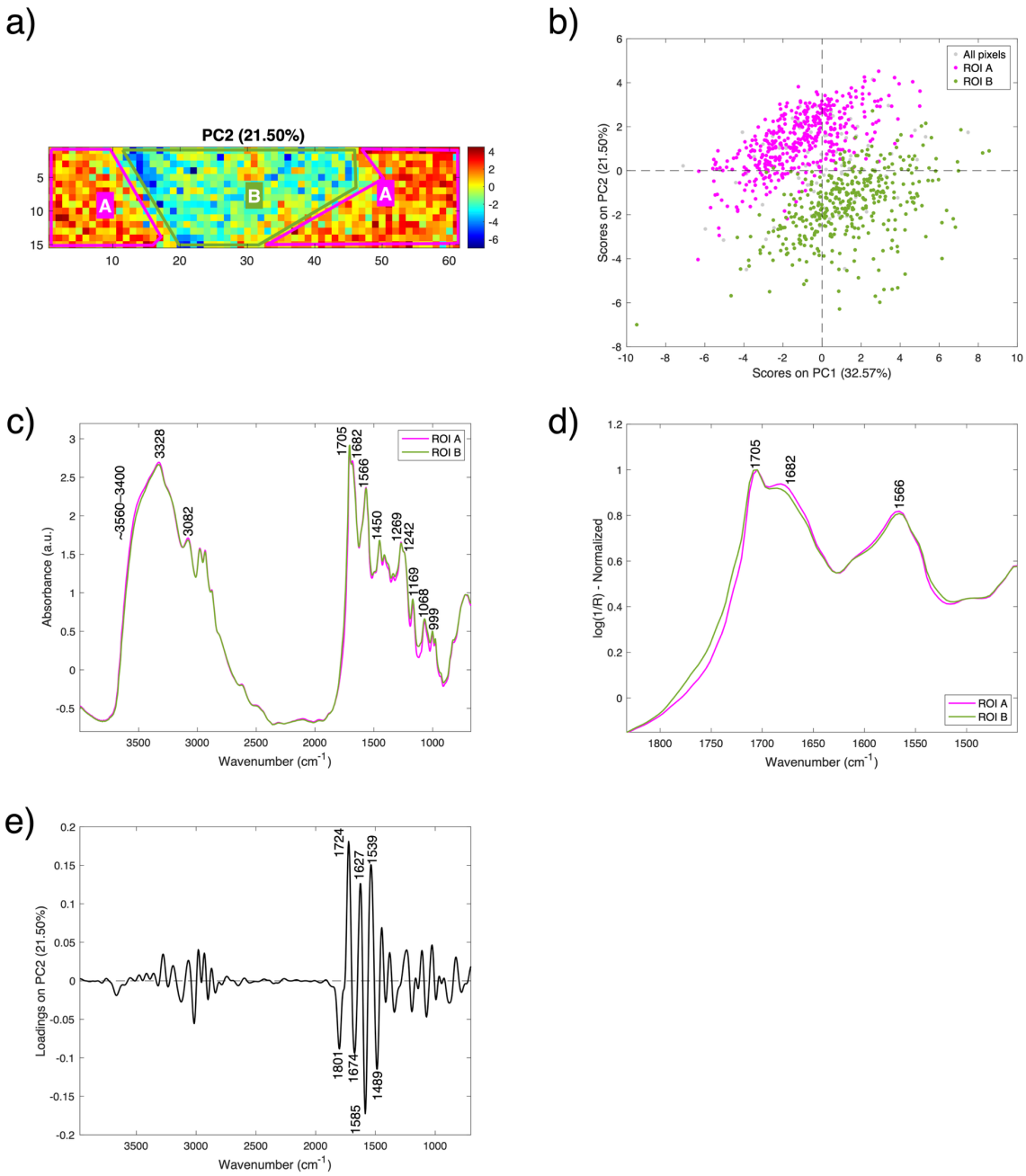

Figure S6. PCA brushing results of S20 on PC2 score map with a focus on selected MIR region (1800–1500 cm^{-1}). (a) PC2 score map brushing areas; (b) highlighted scores in PCA score plot of two clusters: unirradiated area (A); irradiated area (B); (c) corresponding average spectra with (d) normalized region enlargement based on amide I; (e) PC2 loading profile from the second derivative PCA model.

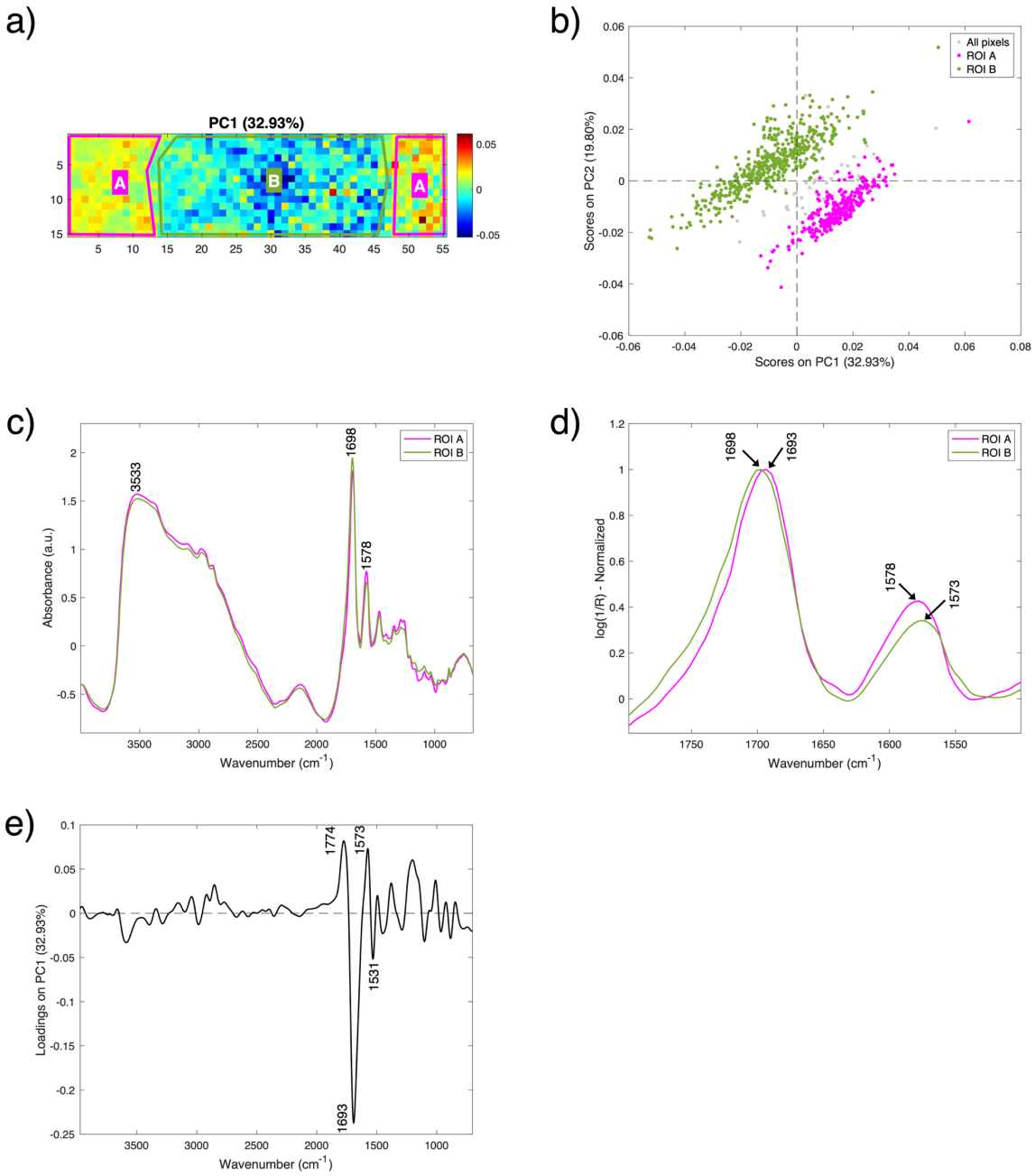

Figure S7. PCA brushing results of P10 on PC1 score map with a focus on selected MIR region (1800–1500 cm^{-1}). (a) PC1 score map brushing areas; (b) highlighted scores in PCA score plot of two clusters: unirradiated area (A); irradiated area (B); (c) corresponding average spectra with (d) normalized region enlargement based on amide I; (e) PC1 loading profile from the first derivative PCA model.

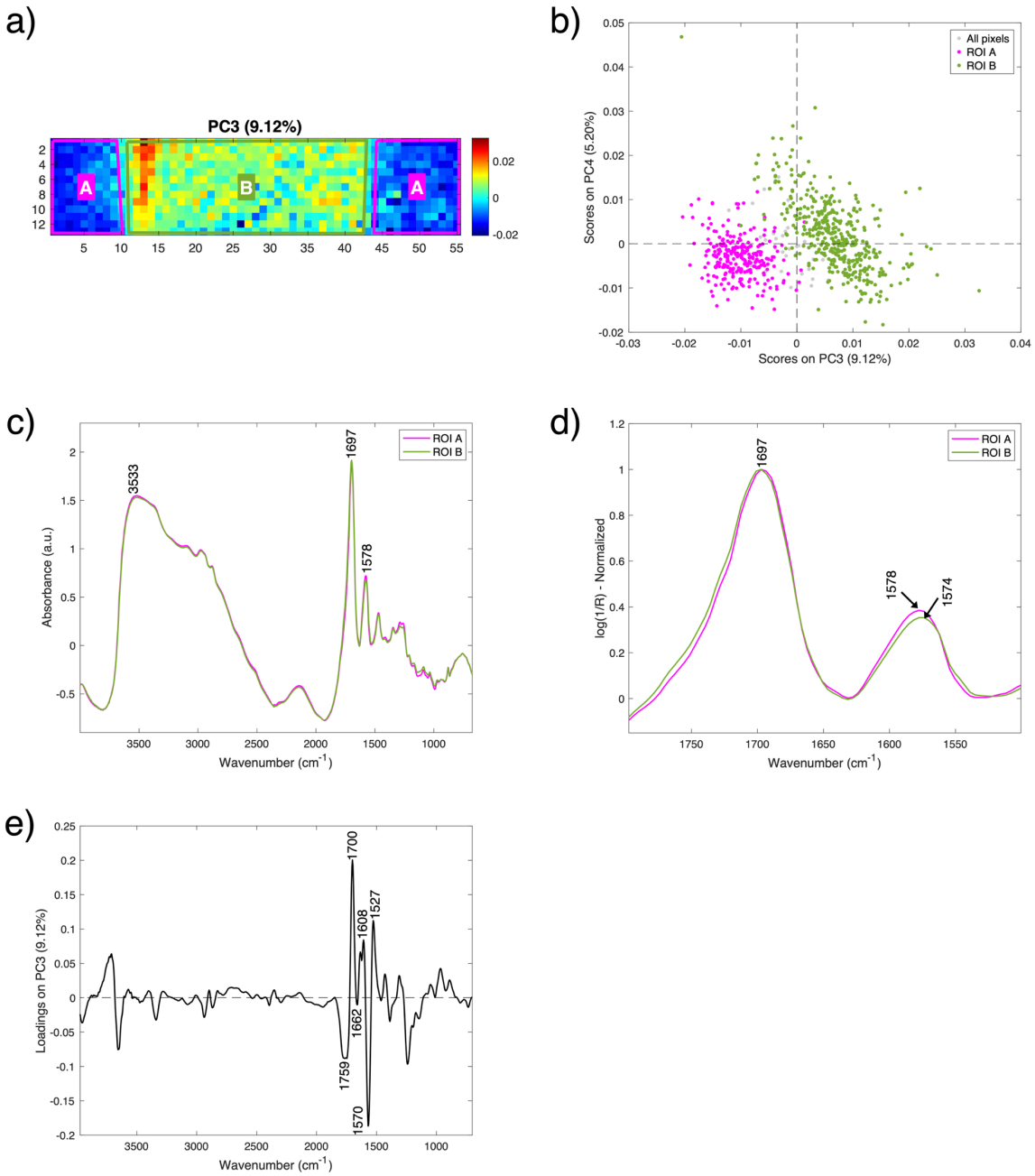

Figure S8. PCA brushing results of P4 on PC3 score map with a focus on selected MIR region (1800–1500 cm^{-1}). (a) PC3 score map brushing areas; (b) highlighted scores in PCA score plot of two clusters: unirradiated area (A); irradiated area (B); (c) corresponding average spectra with (d) normalized region enlargement based on amide I; (e) PC3 loading profile from the first derivative PCA model.

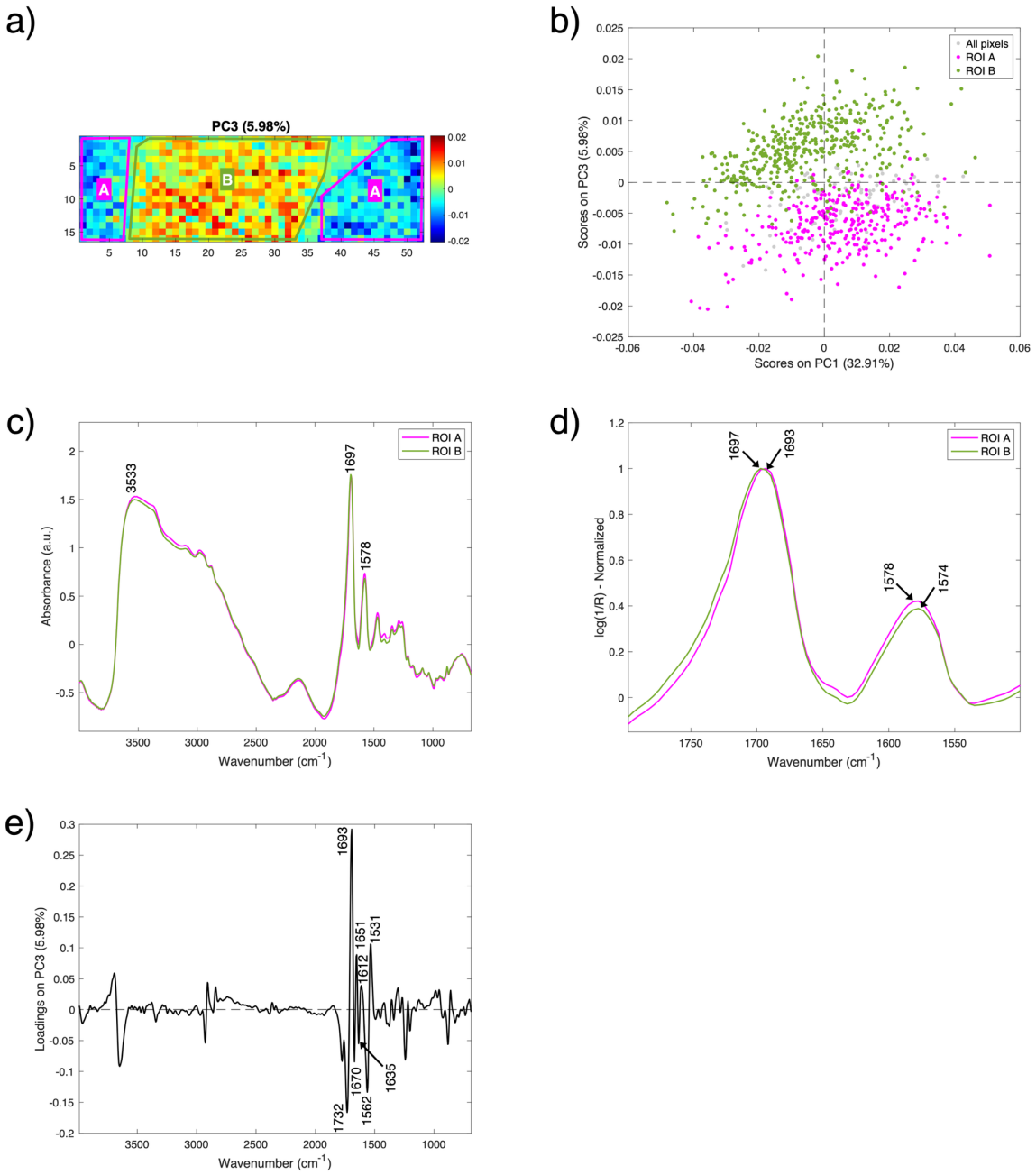

Figure S9. PCA brushing results of P2 on PC3 score map with a focus on selected MIR region (1800–1500 cm^{-1}). (a) PC3 score map brushing areas; (b) highlighted scores in PCA score plot of two clusters: unirradiated area (A); irradiated area (B); (c) corresponding average spectra with (d) normalized region enlargement based on amide I; (e) PC3 loading profile from the first derivative PCA model.

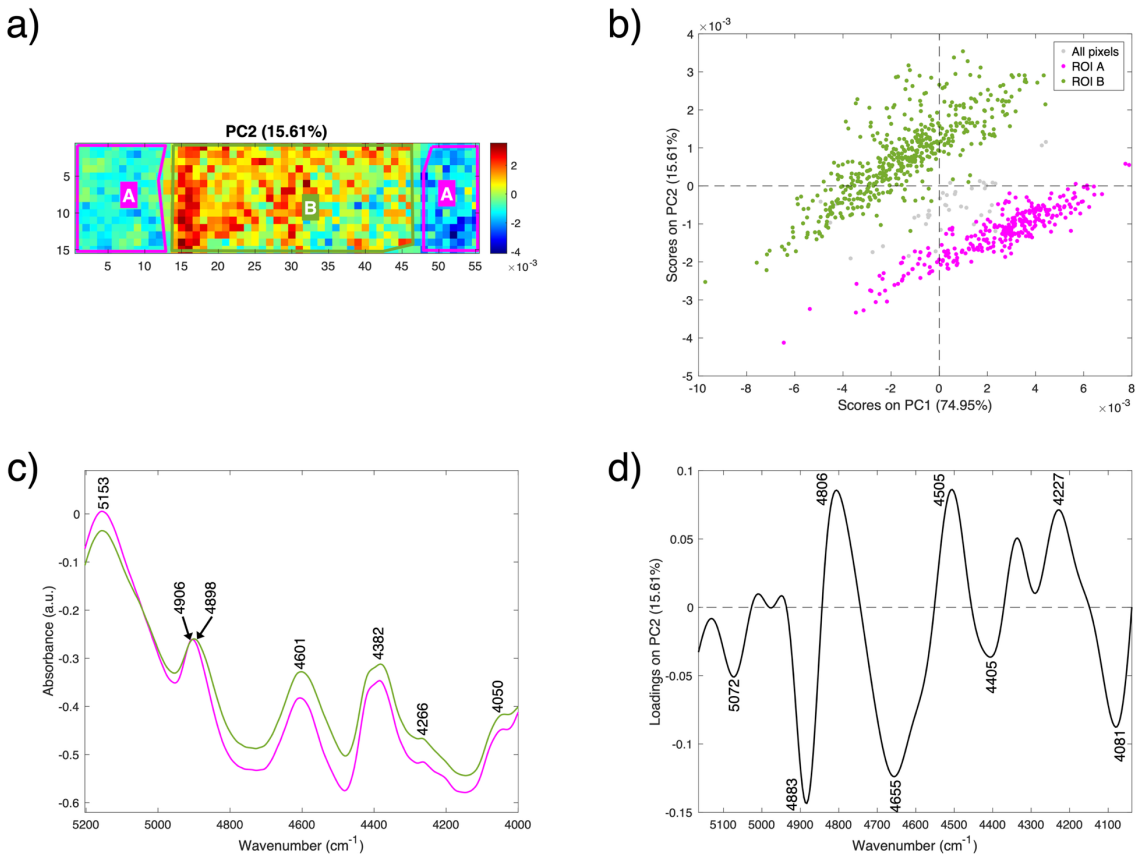

Figure S10. PCA brushing results of P10 on PC2 score map with a focus on selected NIR region (5200–4000 cm^{-1}). (a) PC2 score map brushing areas; (b) highlighted scores in PCA score plot of two clusters: unirradiated area (A); irradiated area (B); (c) corresponding average spectra with (d) PC2 loading profile from the first derivative PCA model.

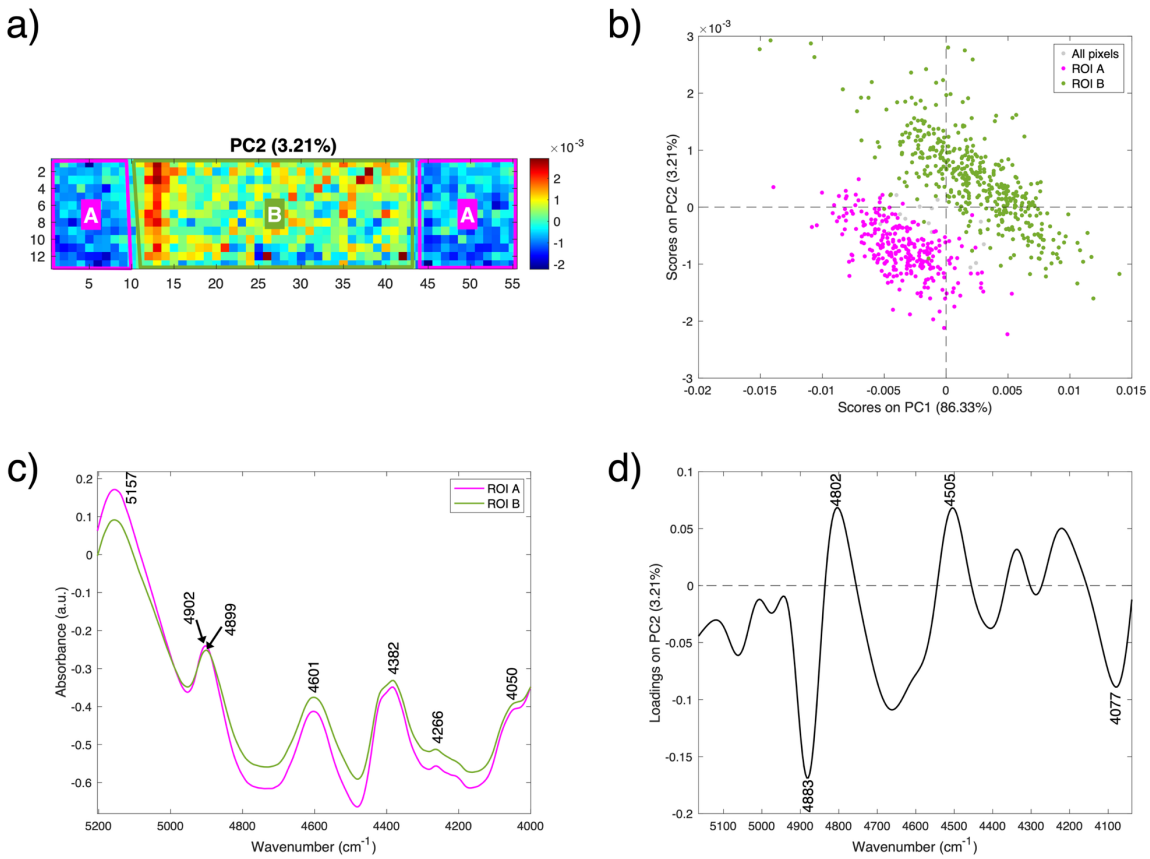

Figure S11. PCA brushing results of P4 on PC2 score map with a focus on selected NIR region (5200–4000 cm^{-1}). (a) PC2 score map brushing areas; (b) highlighted scores in PCA score plot of two clusters: unirradiated area (A); irradiated area (B); (c) corresponding average spectra with (d) PC2 loading profile from the first derivative PCA model.

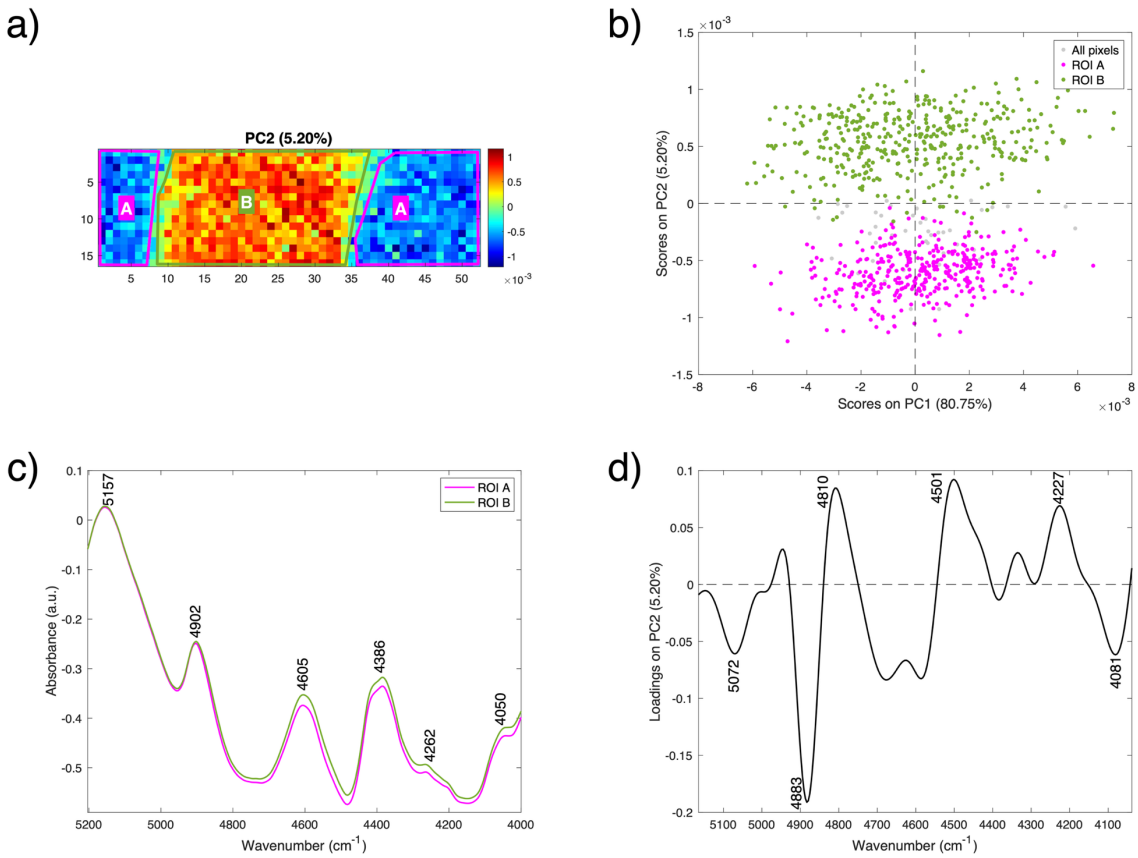

Figure S12. PCA brushing results of P2 on PC2 score map with a focus on selected NIR region (5200–4000 cm^{-1}). (a) PC2 score map brushing areas; (b) highlighted scores in PCA score plot of two clusters: unirradiated area (A); irradiated area (B); (c) corresponding average spectra with (d) PC2 loading profile from the first derivative PCA model.

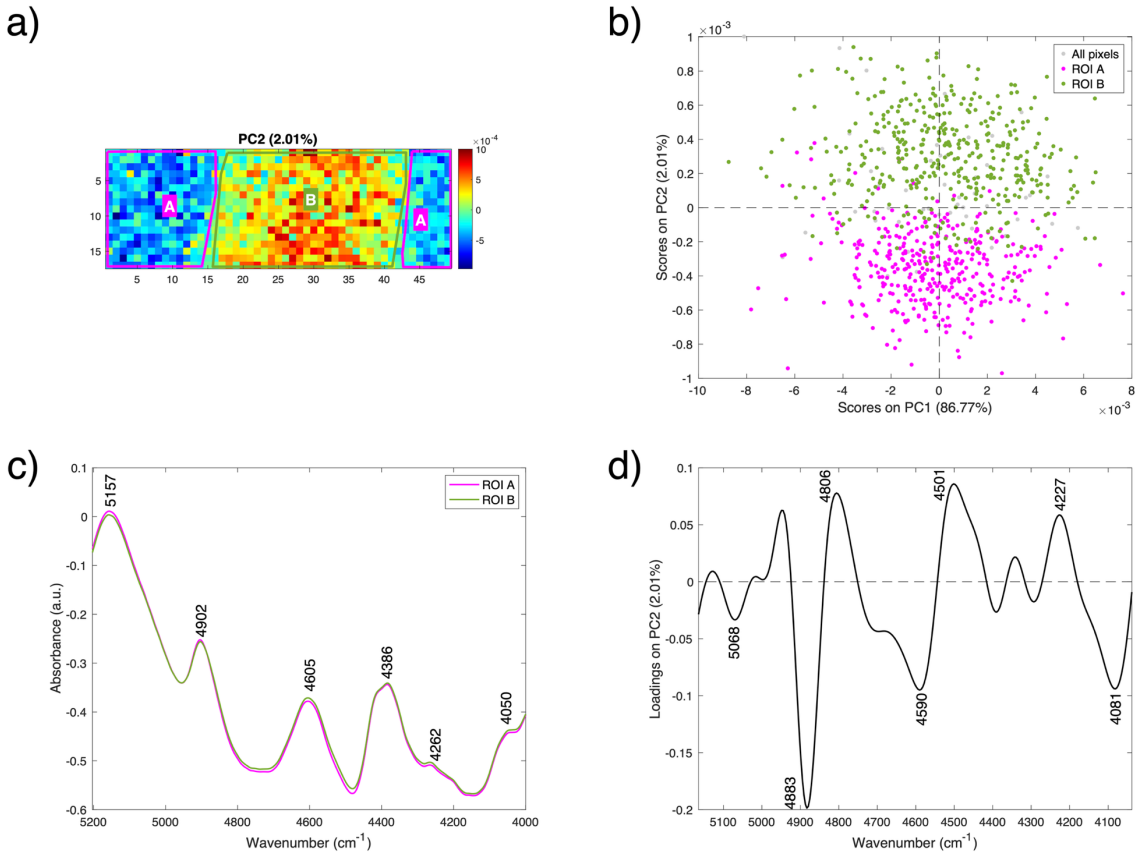

Figure S13. PCA brushing results of P1 on PC2 score map with a focus on selected NIR region (5200–4000 cm^{-1}). (a) PC2 score map brushing areas; (b) highlighted scores in PCA score plot of two clusters: unirradiated area (A); irradiated area (B); (c) corresponding average spectra with (d) PC2 loading profile from the first derivative PCA model.

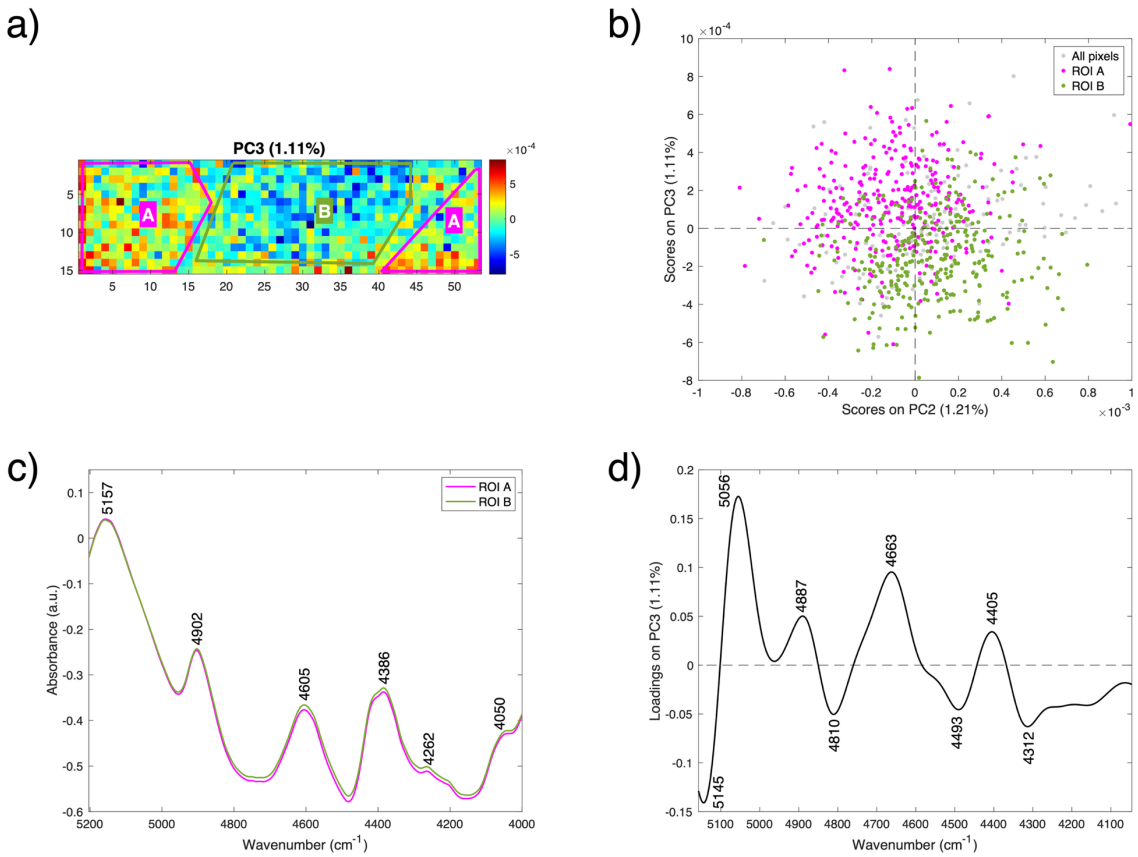

Figure S14. PCA brushing results of P0.5 on PC3 score map with a focus on selected NIR region (5200–4000 cm^{-1}). (a) PC3 score map brushing areas; (b) highlighted scores in PCA score plot of two clusters: unirradiated area (A); irradiated area (B); (c) corresponding average spectra with (d) PC3 loading profile from the first derivative PCA model.

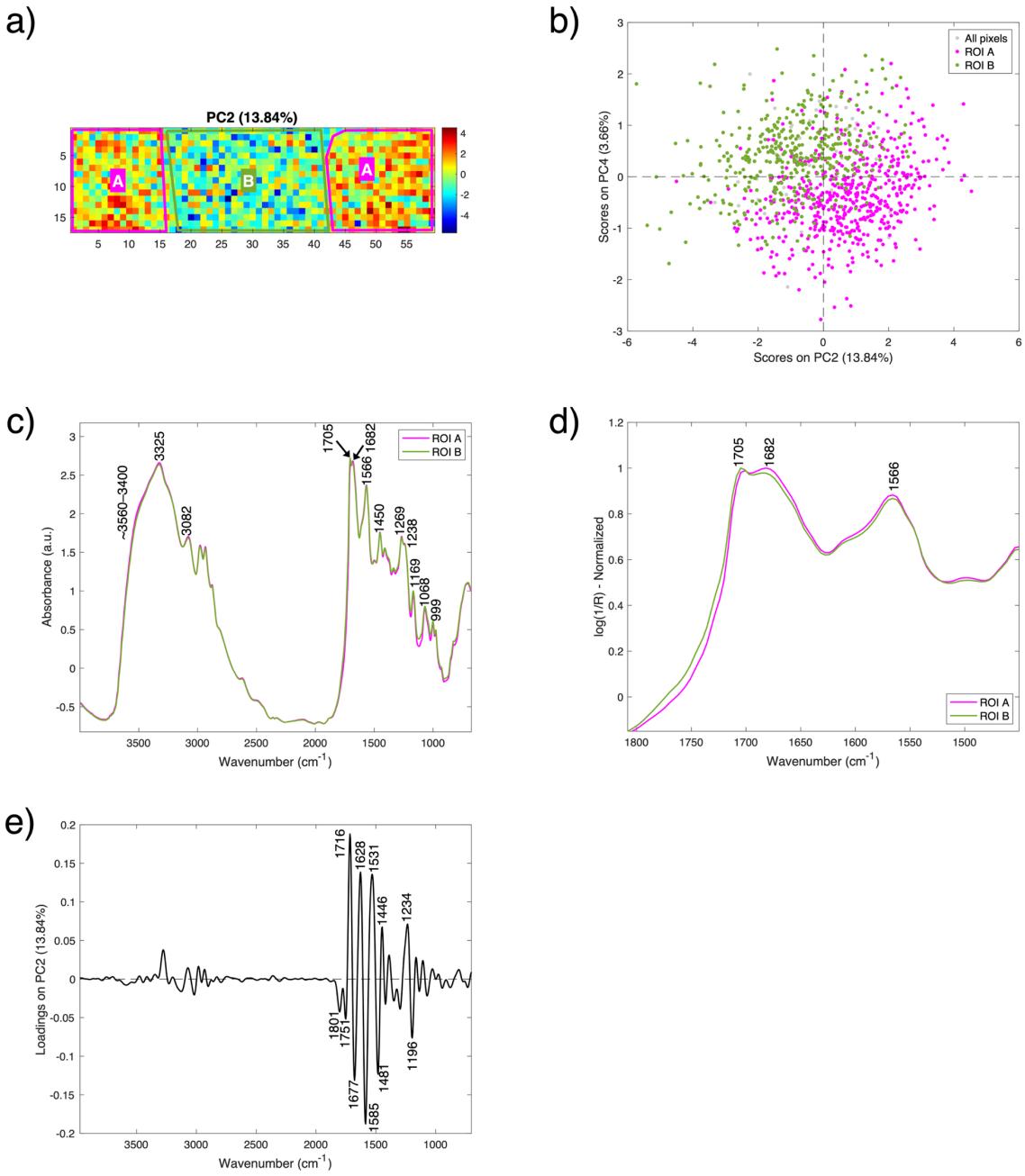

Figure S15. PCA brushing results of S10 on PC2 score map with a focus on selected MIR region (1800–1500 cm^{-1}). (a) PC2 score map brushing areas; (b) highlighted scores in PCA score plot of two clusters: unirradiated area (A); irradiated area (B); (c) corresponding average spectra with (d) normalized region enlargement based on amide I; (e) PC2 loading profile from the second derivative PCA model.

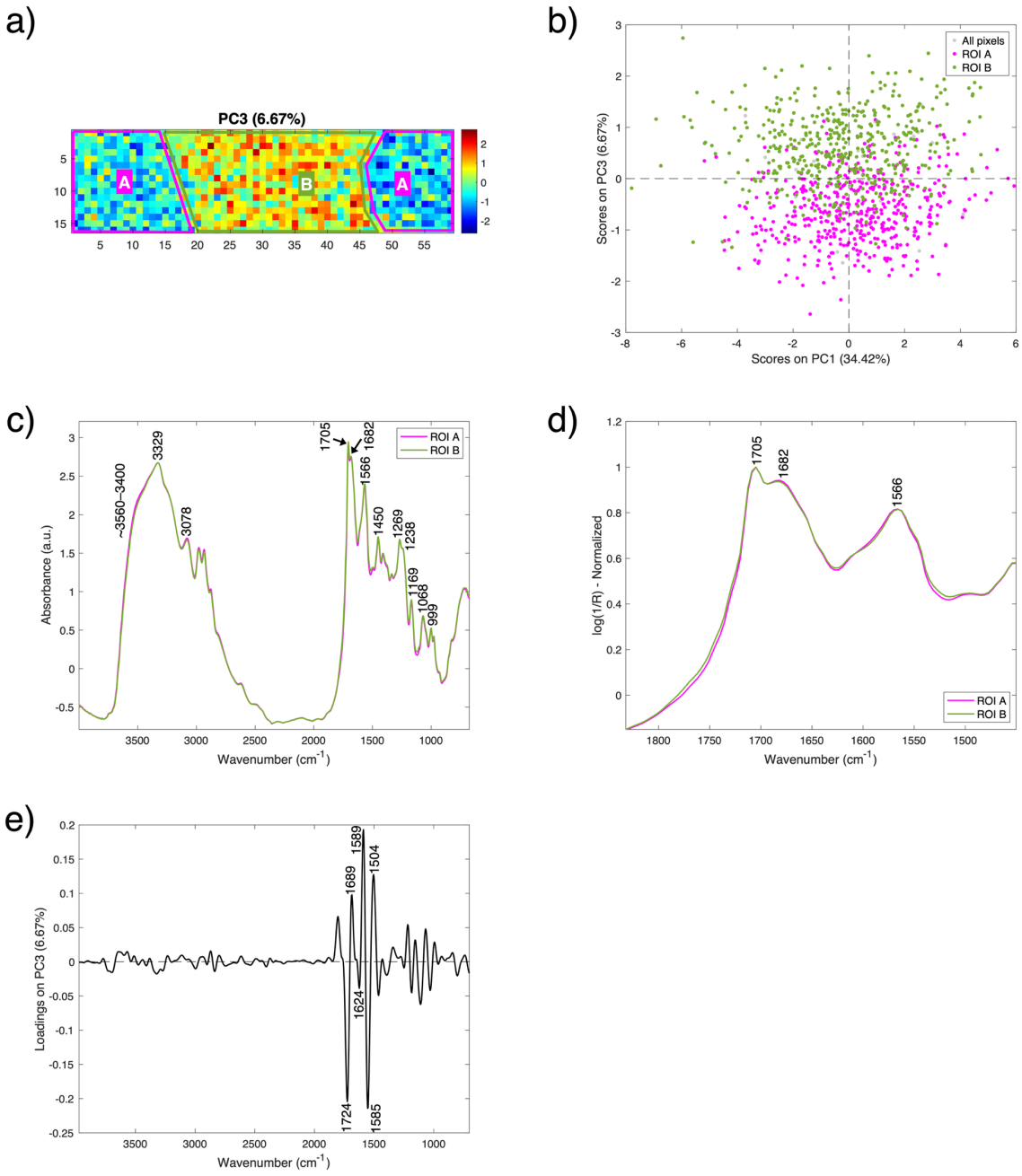

Figure S16. PCA brushing results of S4 on PC3 score map with a focus on selected MIR region (1800–1500 cm^{-1}). (a) PC3 score map brushing areas; (b) highlighted scores in PCA score plot of two clusters: unirradiated area (A); irradiated area (B); (c) corresponding average spectra with (d) normalized region enlargement based on amide I; (e) PC3 loading profile from the second derivative PCA model.

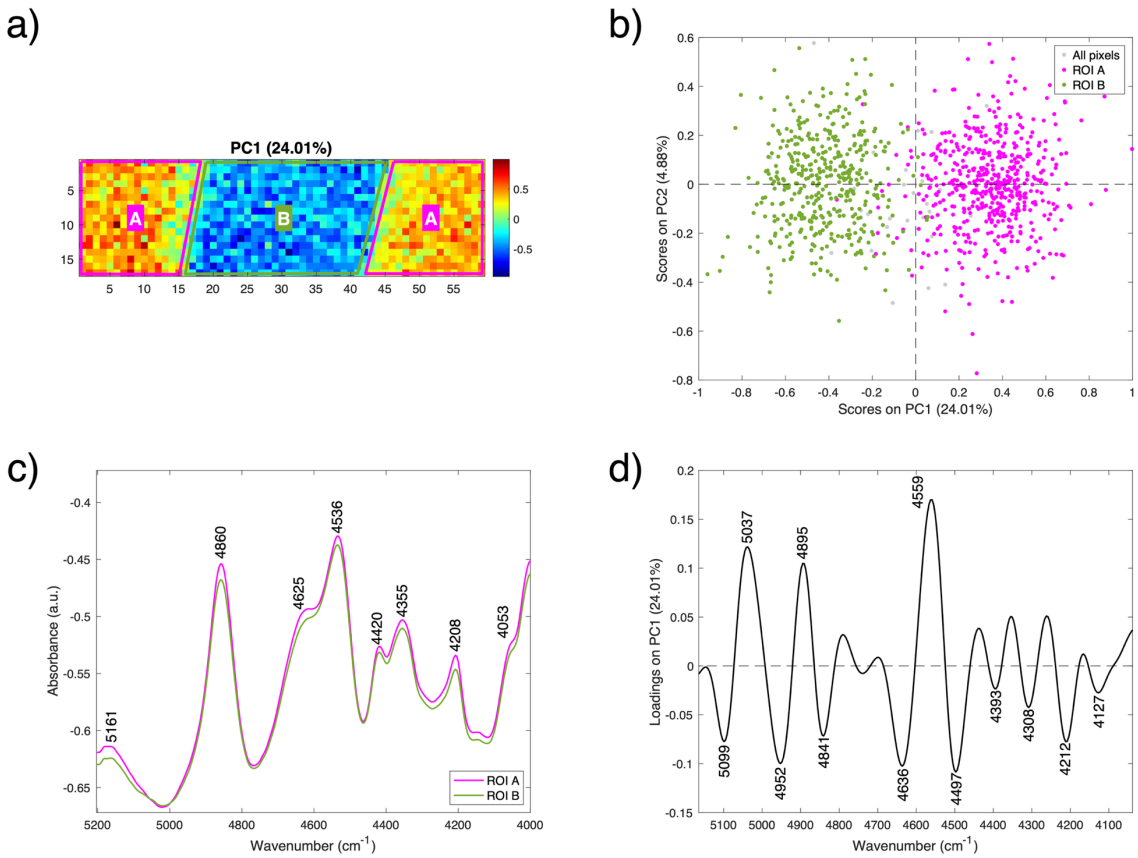

Figure S17. PCA brushing results of S10 on PC1 score map with a focus on selected NIR region (5200–4000 cm^{-1}). (a) PC1 score map brushing areas; (b) highlighted scores in PCA score plot of two clusters: unirradiated area (A); irradiated area (B); (c) corresponding average spectra with (d) PC1 loading profile from the second derivative PCA model.

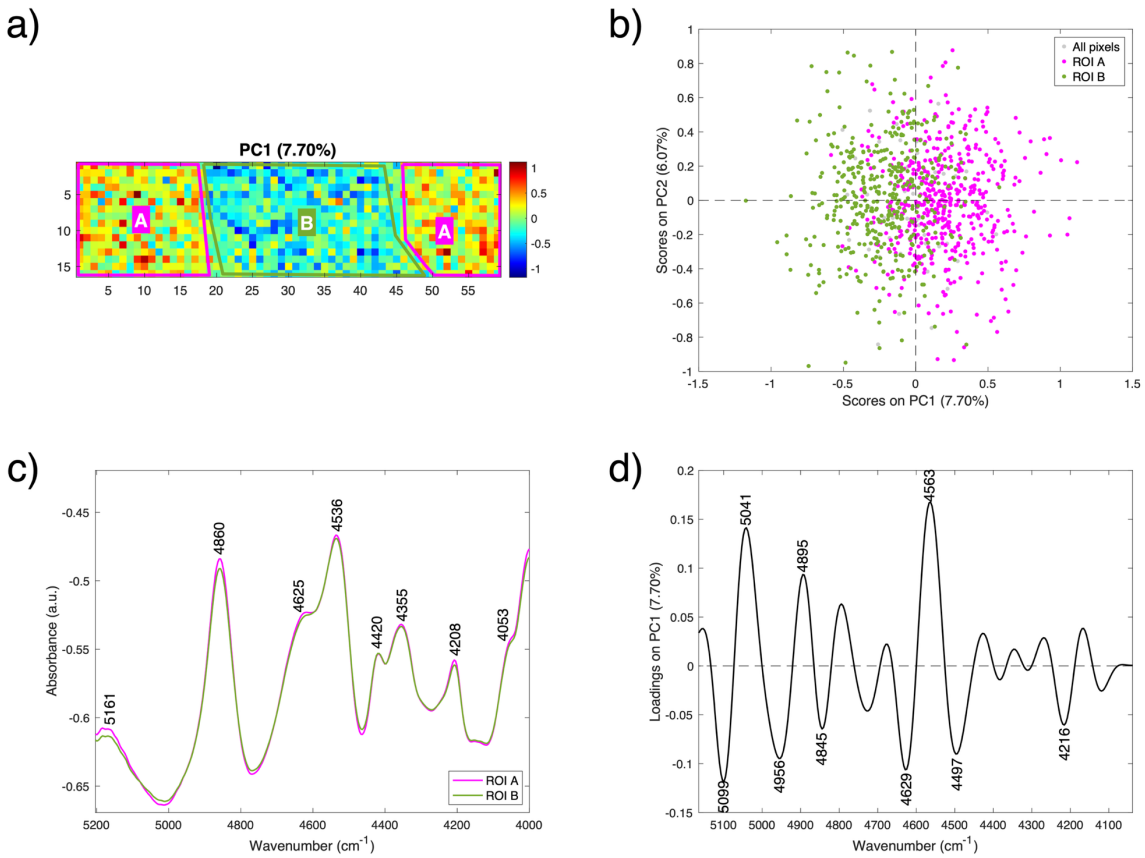

Figure S18. PCA brushing results of S4 on PC1 score map with a focus on selected NIR region (5200–4000 cm^{-1}). (a) PC1 score map brushing areas; (b) highlighted scores in PCA score plot of two clusters: unirradiated area (A); irradiated area (B); (c) corresponding average spectra with (d) PC1 loading profile from the second derivative PCA model.

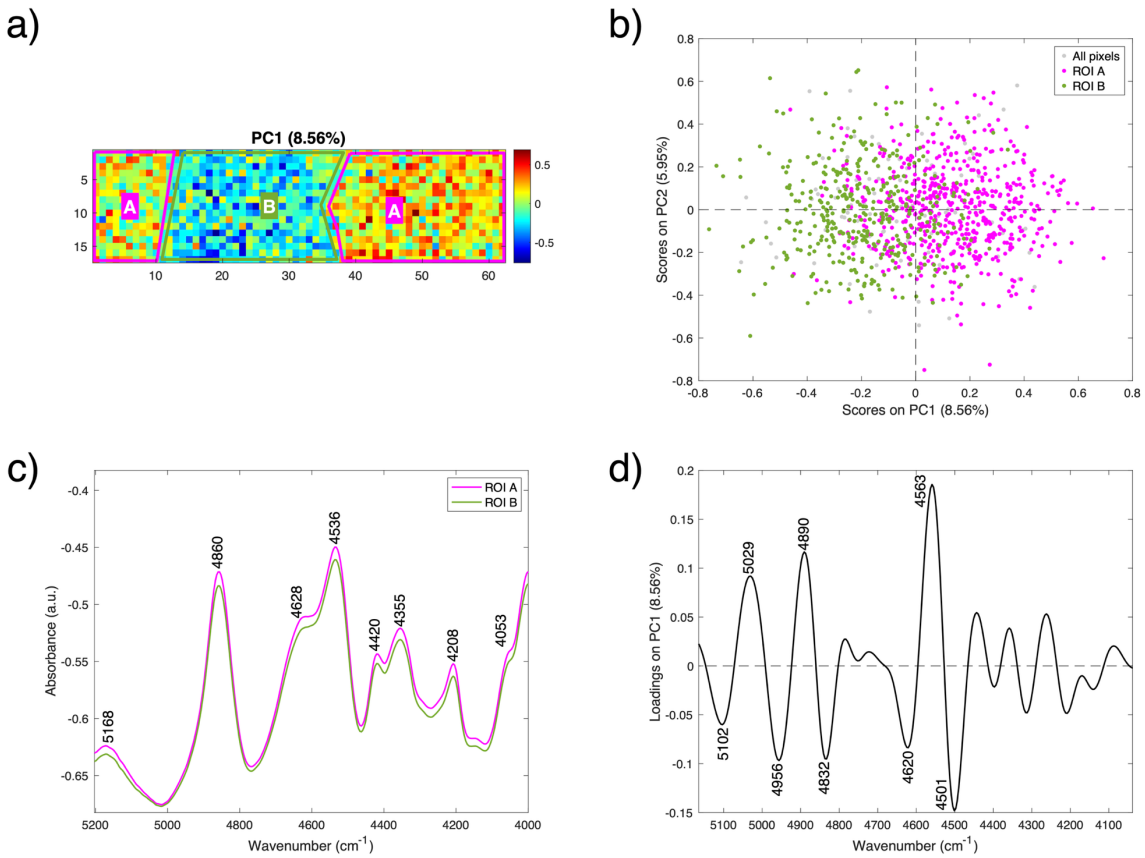

Figure S19. PCA brushing results of S2 on PC1 score map with a focus on selected NIR region (5200–4000 cm^{-1}). (a) PC1 score map brushing areas; (b) highlighted scores in PCA score plot of two clusters: unirradiated area (A); irradiated area (B); (c) corresponding average spectra with (d) PC1 loading profile from the second derivative PCA model.

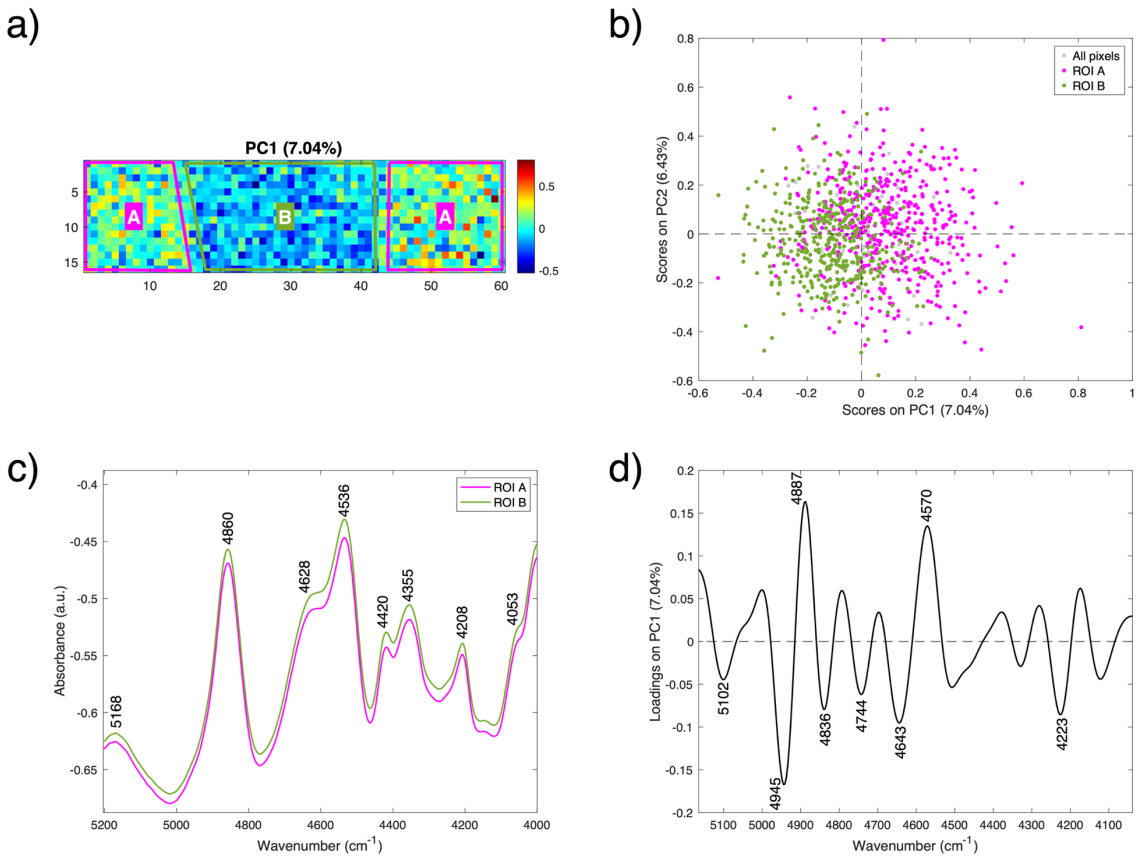

Figure S20. PCA brushing results of S1 on PC1 score map with a focus on selected NIR region (5200–4000 cm^{-1}). (a) PC1 score map brushing areas; (b) highlighted scores in PCA score plot of two clusters: unirradiated area (A); irradiated area (B); (c) corresponding average spectra with (d) PC1 loading profile from the second derivative PCA model.

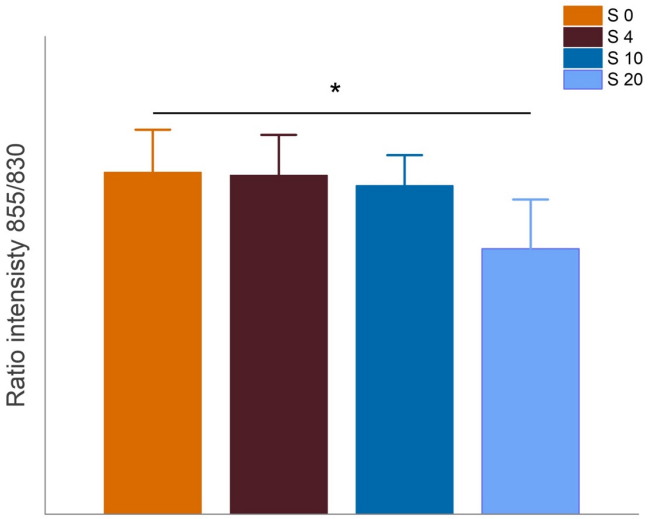

Figure S21. The intensity ratios for the silk samples (S0, S4, S10, and S20), corresponding to doses of 0, 4, 10, and 20 μC/cm², were analyzed using a one-way ANOVA followed by Tukey's post-hoc test. The analysis was conducted with five replicates (n=5) per sample group (p-values reported as follows: * $p < 0.05$, ** $p < 0.01$, *** $p < 0.001$).

Table S1 Band assignments of the main IR absorption bands observed in reflection spectra acquired on parchment (P) and silk (S)

Wavenumber (cm^{-1})	**Assignment**
5170 (S), 5128 (P)	overtone and combination bands of water [1,2]
5000 (P)	NH_2 stretching of the $CONH_2$ group of collagen [2]
4897 (P)	combination band of the stretching and bending modes of NH [3]
4860 (S)	Amide A ν(NH) + amide I/ amide II [1]
4620, 4534 (S)	Amide A ν(NH) + amide III/amide B + amide II [1]
4598 (P)	combination band of amide II and first overtone of carbonyl stretching [3]
4464–4049 (P&S)	combinations of CH stretching and bending modes [4]
3450 (P&S)	stretching of both OH and NH groups variously hydrogen bonded [2]
3300/3320 (P&S)	amide A: NH stretching [1,5]
3080/3070 (P&S)	amide B: NH bending overtone [1,5]
1750–1700 (P&S)	carbonyl compounds formation (oxidation of the polypeptide chains) [5]
1700–1600 (P&S)	amide I: C=O stretching [5]
1580–1510 (P&S)	amide II: NH bending and CN stretching [5]
1300–1180 (P&S)	amide III: a complex mix of NH bending and CN stretching along with deformation vibrations of CH and NH [6]

Table S2. Data pre-treatment methods

Sample	**Full region (7000–675 cm^{-1})**	**NIR (5200–4000 cm^{-1})**	**MIR (4000–675 cm^{-1})**
P20	SNV; Quadratic DT	SG 2-21 [a]; 1st derivative (2-21)[b]	1st derivative (2-15)
P10		SG 2-21; 1st derivative (2-21)	SG 2-15; 1st derivative (2-15)
P4		SG 2-21; 1st derivative (2-21)	1st derivative (2-15)
P2		SG 2-21; 1st derivative (2-21)	1st derivative (2-7)
P1		SG 2-21; 1st derivative (2-21)	1st derivative (2-15)
P0.5		SG 2-25; 1st derivative (2-15)	1st derivative (2-15)
P0.25		SG 2-21; 1st derivative (2-21)	1st derivative (2-15)
P0.125		SG 2-21; 1st derivative (2-21)	1st derivative (2-15)
S20	–	SG 2-21; 2nd derivative (2-21); SNV	SG 2-15; 2nd derivative (2-15); SNV
S10			
S4			
S2			
S1			
S0.5			
S0.25			
S0.125			

[a] Savitzky–Golay 21-point quadratic smoothing.

[b] Savitzky–Golay derivative: window size: 21; polynomial degree: 2

REFERENCES

[1] Geminiani L, Campione FP, Canevali C, Corti C, Giussani B, Gorla G, Luraschi M, Recchia S, Rampazzi L. Historical Silk: A Novel Method to Evaluate Degumming with Non-Invasive Infrared Spectroscopy and Spectral Deconvolution. Materials 2023;16:1819. https://doi.org/10.3390/ma16051819.

[2] Badea E, Miu L, Budrugeac P, Giurginca M, Mašić A, Badea N, Della Gatta G. Study of deterioration of historical parchments by various thermal analysis techniques complemented by SEM, FTIR, UV-Vis-NIR and unilateral NMR investigations. J Therm Anal Calorim 2008;91:17–27. https://doi.org/10.1007/s10973-007-8513-x.

[3] Vagnini M, Miliani C, Cartechini L, Rocchi P, Brunetti BG, Sgamellotti A. FT-NIR spectroscopy for non-invasive identification of natural polymers and resins in easel paintings. Anal Bioanal Chem 2009;395:2107–18. https://doi.org/10.1007/s00216-009-3145-6.

[4] Ricciardi P, Delaney JK, Facini M, Zeibel JG, Picollo M, Lomax S, Loew M. Near Infrared Reflectance Imaging Spectroscopy to Map Paint Binders In Situ on Illuminated Manuscripts. Angewandte Chemie 2012;124:5705–8. https://doi.org/10.1002/ange.201200840.

[5] Derrick M. Evaluation of the State of Degradation of Dead Sea Scroll Samples Using FT-IR Spectroscopy n.d.

[6] Cappa F, Paganoni I, Carsote C, Badea E, Schreiner M. Studies on the effects of mixed light-thermal ageing on parchment by vibrational spectroscopy and micro hot table method. Herit Sci 2020;8:15. https://doi.org/10.1186/s40494-020-0353-z.